Available online at www.sciencedirect.com
ScienceDirect
International Journal of Pharmaceutics 330 (2007) 164–174
INTERNATIONAL JOURNAL OF PHARMACEUTICS
www.elsevier.com/locate/ijpharm

Novel hybrid silica xerogels for stabilization and controlled release of drug

Uroš Maver [a,b], Aljaz Godec [a,b], Marjan Bele [b], Odon Planinšek [a], Miran Gaberšček [b,*], Stane Srčič [a], Janko Jamnik [b]

[a] *Faculty of Pharmacy, University of Ljubljana, Aškerčeva 7m, 1000 Ljubljana, Slovenia*
[b] *National Institute of Chemistry Slovenia, Hajdrihova 19, 1000 Ljubljana, Slovenia*

Received 19 May 2006; received in revised form 8 September 2006; accepted 9 September 2006
Available online 23 September 2006

Abstract

Purpose: The goal was to show that incorporation of a model drug into a porous solid matrix with small enough pores should lead to composites in which the drug would be in the amorphous rather than in the crystalline state. Due to spatial constraints, the amorphous state was expected to be temporally highly stable.
Methods: As a porous solid matrix silica was selected, while nifedipine served as a model drug. The silica–drug composites were prepared using a sol–gel procedure at conditions which yielded pores in the range 2–3 nm. To tune the properties of composites, two silica precursors were combined: tetraethoxysilane (TEOS) and bis-1,2-(triethoxysilyl)ethane (BTSE).
Results: In all composites the amorphous state of nifedipine was proven using several analytical methods. The amorphicity was preserved for at least several months. Drug incorporation into purely TEOS-based silica decreased significantly the release rate. Loosening the structure by addition of BTSE, while preserving the amorphicity, increased the drug dissolution rate. The dissolution behaviour was explained using a combination of the Noyes–Whitney and power law model.
Conclusion: The observed release patterns could be interesting for therapies requiring a high initial drug concentration in blood plasma, followed by a slower release rate of the remaining drug.

Keywords: Amorphous nifedipine; Silica carrier; Dissolution mechanism; BTSE

1. Introduction

During the past decades a diversity of polymer-based pharmaceutical carrier systems for controlling temporal or distributional (site-specific) drug delivery had been developed (Rösler and Vandermuelen, 2001). Pharmaceutical carrier systems offer numerous advantages when compared to conventionally administered drugs in dosage forms, such as improved efficiency and reduced toxicity (Rösler and Vandermuelen, 2001). Typical examples of common drug delivery devices are polymeric cross-linked carrier matrices, such as hydrogels and supramolecular polymer aggregates, as well as different types of microencapsulation vehicles (Rösler and Vandermuelen, 2001). These delivery systems have been widely investigated for sustained and targeted delivery of biologically active substances (Jain and Shah, 1998).

A promising technique for preparation of controlled delivery systems is the sol–gel procedure, which involves the manufacture of an inorganic matrix through the gelation of colloidal suspension (sol) at low temperature and in mild conditions. This technique also allows incorporation of highly sensitive molecules, like proteins and peptides into the gel (Nicoll and Radin, 1997; Santos and Radin, 1999). Examples of successfully prepared materials using the sol–gel technique are silica xerogels intended for sustained and controlled release of ibuprofene (Anderson and Rosenholm, 2004), dexmedetomidine (Kortesuo and Ahola, 2001a) or indomethacine (Watanabe and Wakiyama, 2001). The drug substance incorporated into the sol is distributed

* Corresponding author. Tel.: +386 1 4760 320; fax: +386 1 4760 300.
E-mail address: miran.gaberscek@ki.si (M. Gaberšček).

0378-5173/$ – see front matter © 2006 Elsevier B.V. All rights reserved.
doi:10.1016/j.ijpharm.2006.09.024

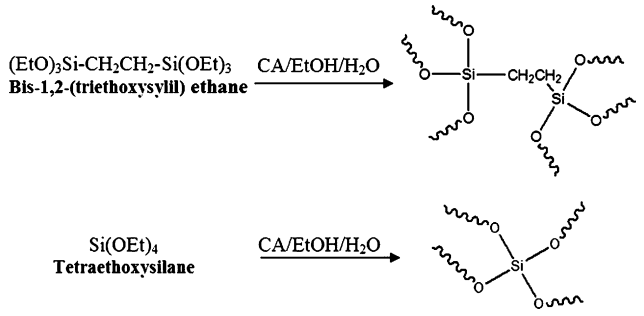

Fig. 1. Schematic presentation of the hydrolysis of the precursors showing the possible growth of the matrix (curved line).

within the porous silica xerogel network. It has been shown that basic drugs release in a sustained manner whereas neutral drugs are released very quickly from silica (Unger and Rupprecht, 1983). Silica causes no adverse tissue reactions and degrades in the body to $Si(OH)_4$, which is eliminated through the kidneys (Kortesuo and Ahola, 2001a).

The composition of the sol, the type and course of reaction, the drying temperature, the pH of the sol and the type and concentration of the catalyst are typical experimental parameters that have influence on the structure and surface properties of silica xerogels prepared by hydrolysis and polycondensation of tetraethoxysilane. Adjusting these parameters allows one to change the profile of drug release (Ro and Chun, 1991; Curran and Stiegman, 1999).

There are three main kinds of silanes. The commonly used silane coupling agents are the so-called functional silanes with a general formula $X_3Si(CH_2)_nY$, where X represents a hydrolysable group, Y an organofunctional group and n the spacer chain length expressed in methylene units. The organofunctional group Y (*e.g.*, –Cl, $–NH_2$, –SH, etc.) is selected so as to display the maximum reactivity or compatibility with the polymer to be bonded subsequently. The group X (*e.g.* $–OCH_3$, $–OCH_2CH_3$ and $–OCOCH_3$) makes the silane prone to hydrolysis to silanols (–SiOH) (Franquet and Biesemans, 2004) (Fig. 1).

Bridged silane coupling agents (a typical example is bis-1,2-(triethoxysylil)ethane—BTSE) lack the organofunctional group Y, which is substituted by a second X_3Si moiety, resulting in structures of the type $X_3Si(CH_2)_mSiX_3$. These molecules are not suitable for polymer adhesion improvement but are appropriate as cross-linking agents (Franquet and Biesemans, 2004) and, as shown in this study, they can be used for tailoring the release of drugs. The third kind of silanes, i.e., bifunctional silanes, is not related to the present investigation.

There are many approaches to the sol–gel synthesis of hybrid materials, most of which involve a combination of two or more precursor species. Addition of organic modifiers is widely used for modifying the morphology and surface characteristics of silica xerogels prepared with the precursor TEOS. Methyltriethoxysilane (MTES) has been used for the synthesis of hydrophobic membranes with a high permeability for gases (Wu and Joo, 2004 and Wu and Joo, 2005). With the addition of methyltrimethoxysilane (MTMS) we decrease the amount of surface silanol groups which results in more hydrophobic surface (Krihak and Shahriari, 1996). These two modifiers have been widely studied for many purposes. Another precursor for hybrid materials is BTSE. It has been used in industrial processes to protect the metal surface against corrosion (Franquet and Biesemans, 2004). It has also been studied as a potential bromide source (Melde and Holland, 1999).

Nifedipine (NIF), 1,4-dihydropyridine with calcium channel blocking activity, has a poor aqueous solubility (Syed Laik, 1989), resulting in low and often irregular bioavailability. However, if we attain a sustained release of NIF, for example, by incorporating it into a porous insoluble matrix, we could achieve an increased effectiveness with less side effects, as shown in the case of intravenous infusion (Breimer and Danhof, 1997). In the present work we study in detail the correlations between the morphological features and release properties of NIF incorporated into porous silica. These correlations should give a solid background for design of specific systems for intravenous infusion of NIF—a subject of further studies.

The materials in this study were synthesized on the basis of thoroughly documented synthesis routes (Wagh and Pajonk, 1997; Wagh and Venkateswara Rao, 1998) with TEOS as the basic silica precursor and BTSE as a modifier. As a model drug substance NIF was used, but we believe that the basic findings may be generalized to other drugs. It should be stressed that Bögershausen and Koller, in press have reported on the preparation and characterization of a range of materials with compositions and structures analogous to those prepared in the present study. In that study, however, the basic TEOS structure was modified with precursors other than BTSE. Also, instead of NIF, Persantin was used as the model drug. Most importantly, Bögershausen et al. did not report any effect of drug encapsulation on its structure (crystallinity versus amorphicity, etc.). By contrast, the focus of the present study is exactly these effects. Our basic hypothesis is that by encapsulating a drug into small enough silica pores, one should be able to suppress the crystal nucleation and growth of the drug. The final silica–drug composite should then contain the drug in its amorphous state. As NIF normally possesses a high degree of crystallinity and its amorphous form is very unstable, it seemed a perfect model drug for testing this hypothesis. The amorphous form of drugs has been interesting for pharmaceutical application due to its specific characteristics, such as a faster dissolution and a higher reactivity when compared to the crystalline form. Of course, when amorphous drug is encapsulated into a solid matrix, these characteristics may be changed. In particular, it is expected that the dissolution rate of drug will be decreased. However, we demonstrate that by appropriate combination of silica precursors (*e.g.*, by selecting an appropriate BTSE/TEOS ratio), we can again increase the average rate of dissolution of the amorphous drug from the silica–drug composites. The mechanisms leading to this increase are discussed in detail. The finding that the dissolution rate of drug can be tailored by appropriate selection of BTSE/TEOS ratio could be used in various applications, as discussed in Section 5.

Table 1
Mole ratios of synthesis precursors for different xerogel formulations

	TEOS	BTSE	H_2O	EtOH	CA	NIF
SCN1	1	0	7	5	0.1	0.019
SCBN1	1	0.05	7	5	0.1	0.019
SCBN2	1	0.1	7	5	0.1	0.019
SCBN3	1	0.2	7	5	0.1	0.019
SCBN4	1	0.3	7	5	0.1	0.019
SCBN5	0	1	7	5	0.1	0.019

2. Materials and methods

2.1. Preparation

2.1.1. Preparation of nifedipine-doped hybrid silica xerogels

Silica sols were prepared at 60 °C by acid hydrolysis and polycondensation of TEOS (Merck), BTSE (ABCE GmbH) with distilled water (H_2O), ethanol (EtOH, Riedel de Häen), citric acid (CA, Aldrich) and NIF (Lek). The samples contained different amounts of BTSE as shown in Table 1.

NIF was dissolved in a mixture of TEOS, BTSE, H_2O, EtOH and CA to form a clear hydrolyzed sol. Ultrasound homogenizer was used to homogenize the sol after the addition of CA and NIF to the sol.

It is known that, when exposed to light, NIF decomposes to nitroso- and nitro-derivatives (Budvári-Báráni and Szász, 1990). For this reason all procedures were carried out under light-protected conditions.

The prepared sol was poured into dark vials wrapped into aluminous foil to prevent aromatization of NIF. After the gelation, the samples were additionally dried for 2 days at 60 °C. Mole ratios of compounds used for preparation of different xerogel formulations are shown in Table 1.

The hydrolysis of the precursors is schematically shown in Figs. 1 and 2.

2.2. Characterization procedures

2.2.1. Specific surface area and porosity parameters

Specific surface area and porosity parameters were determined using the Brunauer–Emmet–Teller (BET) technique based on nitrogen gas adsorption (TRISTAR 3000). Prior to analysis, the samples were crushed and outgassed.

2.2.2. X-ray diffraction

X-ray diffraction measurements were carried out on crushed samples using a Siemens D-5000 diffractometer with Cu Kα radiation at 40 kV and 30 mA.

2.2.3. Thermal analysis

The crushed samples were analyzed by differential thermal analysis (DTA) and thermal gravimetric analysis (TG) (NETZSCH STA 409C/CD) from room temperature (293 K) to 1183 K in air conditions with a rate of temperature increase of 10 K/min.

2.2.4. Scanning electron microscopy (SEM)

Dried samples for scanning electron microscopy were ground and pressed on a double-sided adhesive carbon tape (SPI Supplies, USA). Then the samples were imaged with a field emission scanning electron microscopy (FE-SEM, Supra 35 VP, Carl Zeiss, Germany) operated at 1 keV.

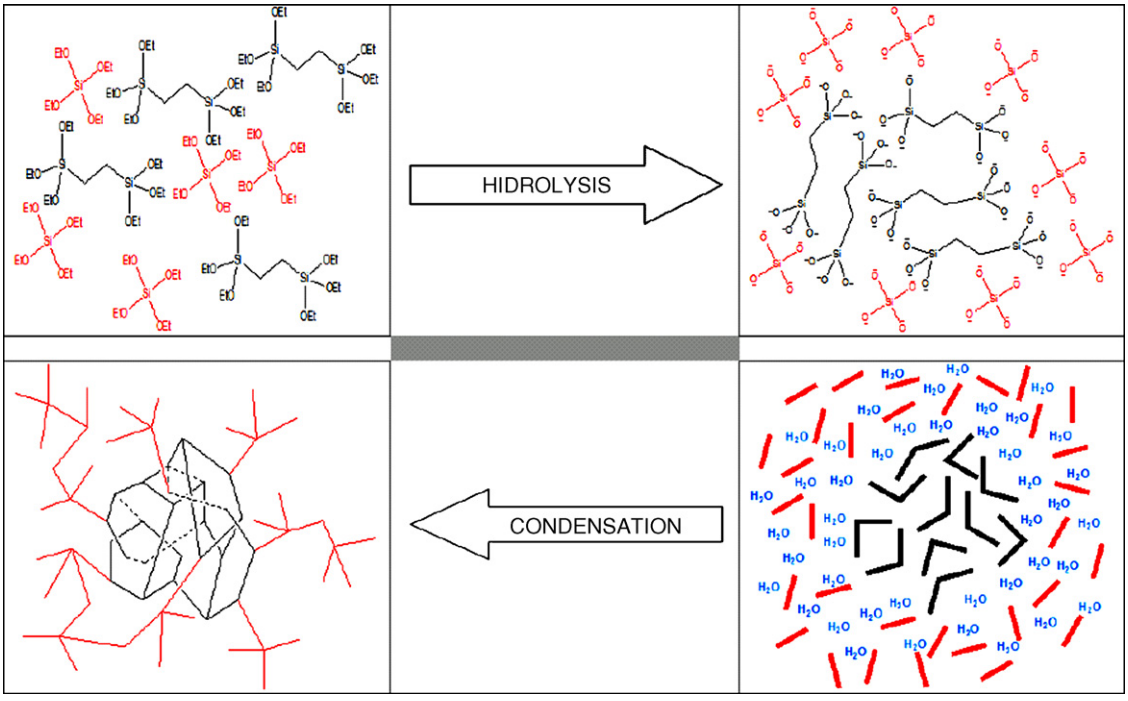

Fig. 2. Schematic presentation of hydrolysis and condensation leading to formation of primary particles in an aqueous milieu (TEOS: red, BTSE: black). (For interpretation of the references to colour in this figure legend, the reader is referred to the web version of the article.)

2.2.5. Drug release and analysis

Dissolution studies of NIF from crushed samples were performed using the USP XXV paddle method (Vankel 7000 Dissolution test station, USA) with a stirring speed of 100 rpm. All samples were sown prior to dissolution. For the analysis, the size fraction between 1000 and 800 μm was used. Phosphate buffer solution with pH 6.8, containing 0.5% sodium lauryl sulphate, was used as a dissolution medium, assuring sink conditions ($C < 0.15C_S$). Samples containing ca. 10 mg of NIF were dissolved in 900 mL of dissolution medium at 37.0 ± 0.5 °C. At appropriate time intervals, aliquots of 10 mL were withdrawn and measured spectrophotometrically (UV Spectrophotometer 8453, Hewlett Packard, Germany) at λ = 238 nm. The experiments were carried out in duplicate, therefore only mean values with S.D. error bars are reported.

2.2.6. Particle sizing

To get a clearer insight into dissolution mechanism we used, apart from spectrophotometry, also particle sizing as a method for particle dissolution studies. The average particle size was measured using a Malvern Mastersizer 2000 laser diffraction instrument. To assure the same conditions, all samples were crushed and sown before carrying out the experiments. To appropriately simulate the dissolution process, we used the same size fractions (1000–800 μm) as in the drug release experiments.

2.2.7. Infrared spectroscopy

The FTIR analysis was performed using a Perkin-Elmer System 2000 spectrometer. Data were acquired using Spectrum software (Version 3.01, Perkin-Elmer LLC Co.). The spectra were measured over the range 4000–650 cm^{-1} with an instrument resolution of 4 cm^{-1}. Each individual spectrum was an average of 36 scans. Dried samples were crushed prior to measuring.

3. Results

Theoretical percentage of NIF in the dried xerogels, as calculated from the initial amounts of used precursors, is shown in Table 2. In all gels the content of NIF was such that, after drying, the samples contained the therapeutic dosis of NIF (5–13 wt%).

Regardless of the composition of prepared xerogels, X-ray diffractograms show no sharp peaks indicative of the presence of a crystalline form (Fig. 3).

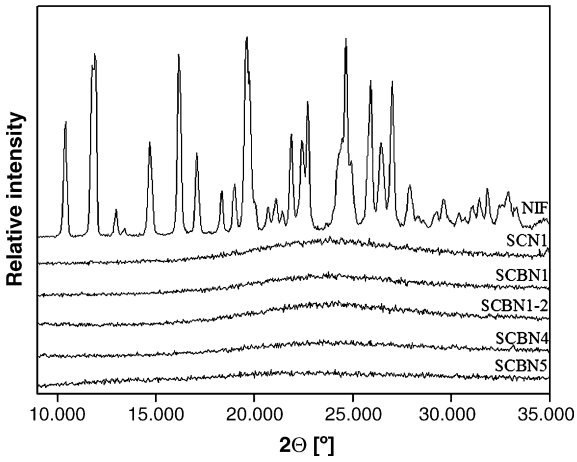

Fig. 3. X-ray diffractograms of the prepared xerogels.

Examination using scanning electron microscopy at high magnification showed that all samples exhibited a rough surface on a nanometre scale (Fig. 4). This implies the presence of nano-sized pores. Indeed, N_2 adsorption experiments showed an average pore diameter of about 2.4 nm (Table 2). Visual examination, in combination with a low magnification SEM observation, showed that, after using the same crushing procedure, the modified samples SCBN*x* (*x* = 1–4) contained particles with dimensions between 10 and 100 μm while the nonmodified sample SCN1 consisted of particles of a few 100 μm in size (Fig. 5). The typical particles size in sample SCBN5 determined from SEM micrographs (not shown) was between 10 and 30 μm.

With increasing BTSE content the dried samples became increasingly more brittle. This effect was initially observed during crushing of samples, where a smaller force had to be exerted to crush the samples with a higher BTSE content. Consistently, the more brittle samples, i.e., those containing more BTSE, disintegrated into a larger number of particles than those containing less BTSE.

N_2-adsorption experiments revealed that addition of small amounts of BTSE (up to 10%) decreased the specific surface area if compared to the nonmodified sample SCN1 (Table 2), which could not be explained based on the available information about the structure of silica-based matrices. However, upon further addition of BTSE, the specific surface area increased significantly and peaked at a value of about 174 g/m^2, which is more than twice the value of the nonmodified sample (80 g/m^2). It is interesting that while the addition of BTSE had a significant

Table 2
Amount of added nifedipine, percentage of nifedipine in the dried xerogels, specific surface area and average pore size of prepared xerogels with different amount of added BTSE

	Amount of nifedipine in the wet sol (g)	Percentage of nifedipine in the dried xerogels (%)	Average pore size (nm)	Specific surface area (m^2/g)
SCN1	0.5	11.2	2.44	80.20
SCBN1	0.5	7.8	2.40	61.63
SCBN2	0.5	8.5	2.31	158.65
SCBN3	0.5	5.0	2.40	174.26
SCBN4	0.5	9.1	–	151.33
SCBN5	0.5	12.8	2.47	58.71

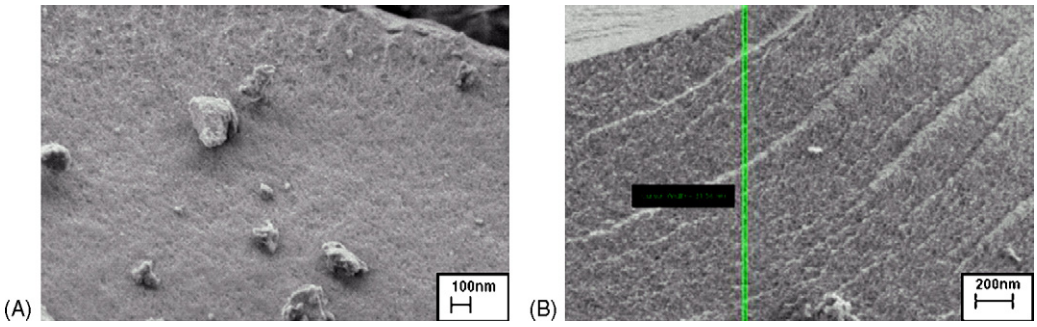

Fig. 4. Scanning electron micrographs of the prepared silica gel xerogels. (A) SCBN1 (BTSE/TEOS mole ratio of 0.05) and (B) SCBN5 (only BTSE was used as a precursor).

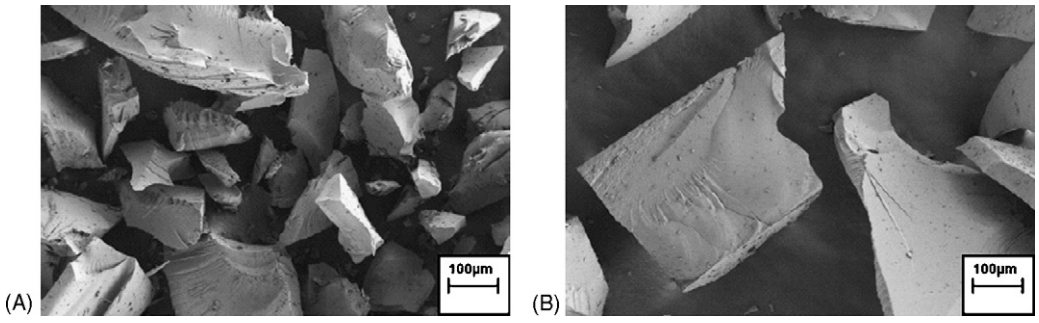

Fig. 5. Scanning electron micrographs of samples after the same crushing procedure. (A) SCN1 (only TEOS was used as a precursor) and (B) SCBN3 (BTSE/TEOS mole ratio was 0.2).

impact on the specific surface area, it did not affect the average pore size (Table 2). This effect can be correlated to the structure of primary particles determined, for example, using a minimization procedure (we used an MS Modeling software). It can be shown that the primary particles (cyclic hexamers) made of BTSE molecules include more free space compared to the primary particles made of TEOS (Fig. 6). This fact could explain, at least partly, the increasing surface area with increasing BTSE/TEOS mole ratio. Based on the structure minimization, we further expected that the BTSE-rich regions would contain additional micropores (pores with sizes < 1 nm). However, such micropores could not be detected experimentally—due to limitations of the N_2 adsorption method. As the molar ratio BTSE/TEOS reaches 0.3 (in sample SCBN4), the surface area starts slightly to decrease. This is probably due to structural mismatches resulting from the fact that BTSE can only grow in three directions as opposed to TEOS (four-direction growth). Apparently, in SCBN4 these mismatches are large enough to cause a partial collapse of the matrix structure. This collapse can probably also expain the faster gelation of these samples (shorter distances between sylanol groups and, therefore, a faster condensation). Because the source of silica for the sample SCBN5 is BTSE only, it could be speculated that the decrease of surface area is due to a denser packing of equal primary particles. By contrast, this is not expected in less ordered structures containing mixed types of primary particles, but further studies are needed to confirm such a scenario.

DTA and TG curves of the as-prepared samples with different BTSE/TEOS ratios are shown in Fig. 7. Each DTA curve exhibits two endothermic peaks occurring between 50–120 and 190–250 °C, respectively. The former peak is ascribed to evaporation of H_2O and EtOH (physically adsorbed and free) (Yang and Choi, 1999). The position of this peak matches with the first loss of mass (7–10%) in TG curves which has also been

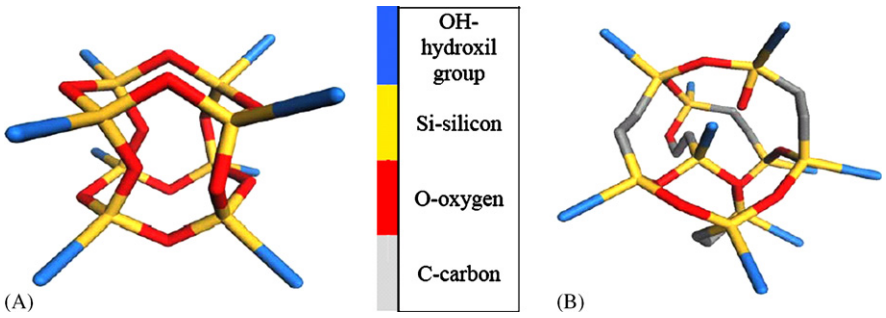

Fig. 6. Scheme of the presumably formed primary particles (cyclic hexamers) made of (A) TEOS and (B) BTSE.

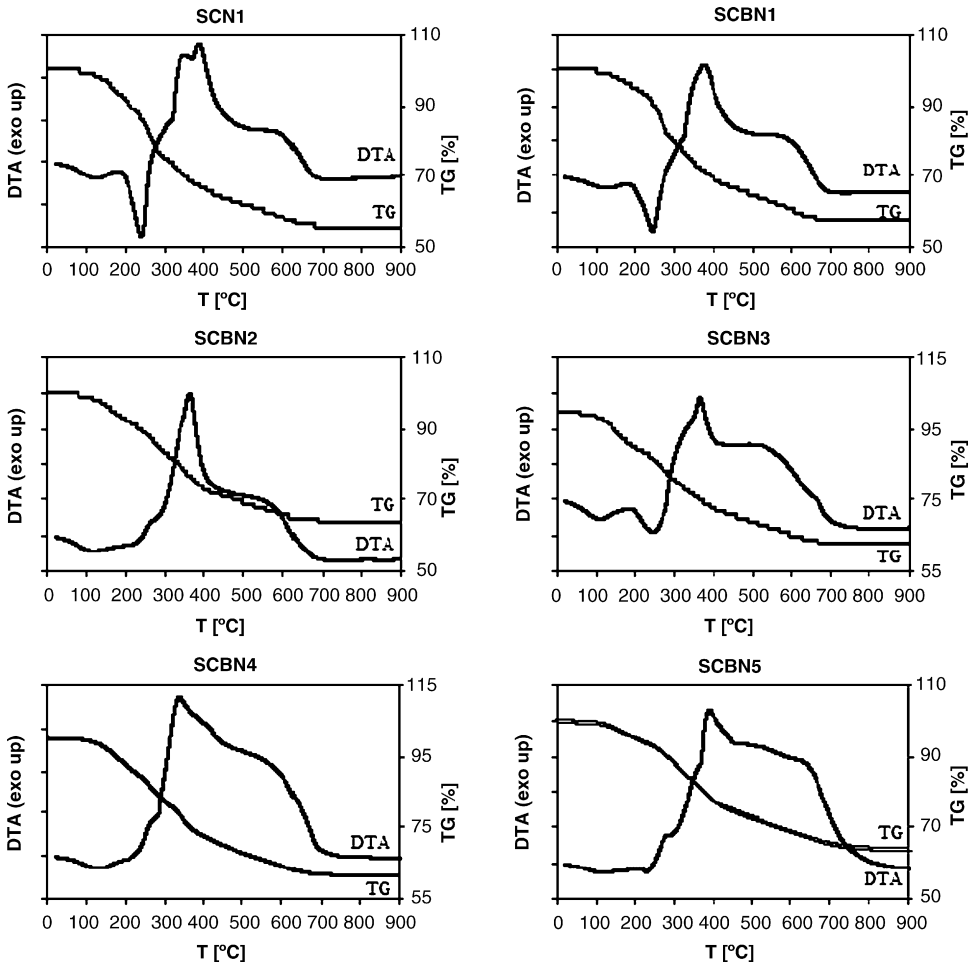

Fig. 7. Results of thermal analysis (DTA and TG) of the prepared samples.

attributed to the evaporation of water and ethanol (22). The second DTA peak (190–250 °C) and the mass loss of 10–15% between 190 and 200 °C correspond to removal of the remaining ethoxy groups (–OEt) and polymerization of the residual SiOH groups (Brinker and Scherer, 1990 and Hu and Mackenzie, 1992).

Most importantly, none of the DTA curves exhibits an endothermic peak between 172 and 174 °C, which is the melting point of NIF (The MERCK Index). This is a strong indication that in all present samples NIF is in the amorphous state.

Sample SCBN1-5 exhibits lower mass losses in the first two regions than the other samples. We ascribe this effect to a higher hydrophobicity of this sample. This means that it adsorbs less H_2O (lower mass loss in the first region) and that less SiOH groups are formed on its surface (lower mass loss in the second region).

The mass loss of 10–15% at temperatures higher than 300 °C is due to combustion of organic components in the xerogel (ethylene bridges in BTSE, NIF, and residual CA) (Brinker and Scherer, 1990). As SCN1 contains no BTSE (no ethylene bridges), the corresponding TG curve exhibits the smallest weight loss in this region. Consistently, as the BTSE content increases, the mass loss also increases. Only in the case of sample SCN1, the exothermic peak due to combustion of the organics is split. Note that this sample has a simpler composition than the other samples (it contains no BTSE and thus no ethylene bridges). As in samples that do contain BTSE no such split is observed, we assume that combustion of the ethylene bridges due to BTSE occurs exactly at the split temperature so that the split itself is hidden.

FTIR spectra in the absorbance mode are depicted in Fig. 8. The absorbance was measured over the range 4000–650 cm^{-1}, but in the present study we focus mainly to the range 1300–850 cm^{-1}, which contains information about the degree of condensation (Si–O–Si bridges) and the presence of –SiOH groups on the surface. While the former may affect the mechanical properties of the samples (see Section 4), the latter determine the surface wettability of silica which may have influence on overall silica–drug interactions.

Possible distractions caused by the presence of various substances within the composites (NIF, EtOH, CA) were excluded by comparing appropriate samples prepared with and without these substances.

In the range of the present analysis, the bands due to Si–O–Si bridges appeared at 1200 and 1080 cm^{-1}. The absorbances of these peaks could be partly affected by the presence of EtOH (bands at 1080 and 1047 cm^{-1}). SiOH bands appeared at 950 cm^{-1}. The band at 1270 cm^{-1} exhibits the presence

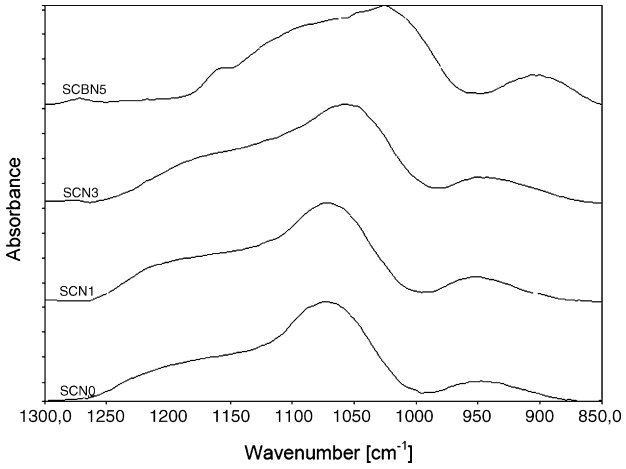

Fig. 8. FTIR spectra of the prepared samples. The composition of the measured samples (SCN0, SCN1, SCBN3 and SCBN5) is given in Table 2.

of methylene species—because the BTSE molecule can be regarded as two MTES (methyltriethoxysilane) molecules connected over two methyl species. So, the intensity of this band increases with the increasing amount of added BTSE. As the BTSE/TEOS ratio is increased, the peaks shift to lower wave numbers. The spectrum for SCBN5 (containing only BTSE) has a different shape if compared to the other spectra. It exhibits a new peak at 1412 cm^{-1}, the shape of associated peak at 1200–980 cm^{-1} is changed significantly and the peak at 700 cm^{-1} has a higher intensity than in other samples.

Prior to the dissolution/release analysis, all samples were crushed. As expected, dissolution of pure amorphous NIF was found to be slightly faster (within 10%) than dissolution of crystalline NIF. Embedment of NIF into a nonmodified xerogel decreases significantly the percentage of dissolved NIF at all times studied (Fig. 9a). However, with increasing content of added BTSE, the percentage of released NIF again gradually increases (compare the curves in Fig. 9a). A closer analysis shows that the curves for the modified samples can be reasonably divided into two regions: a first region enclosing the period from 0 to about 5 min with a rapid drug dissolution (the so-called burst effect), followed by a second region with a considerably slower average dissolution rate. The initial dissolution rate of modified samples is comparable to the initial dissolution rate of free NIF. This is easiest seen by comparing the curve for sample SCBN5 with the curve for pure NIF in Fig. 9a. After 5 min the curves still have the same values; from this point on, however, the dissolution of both samples proceeds in a considerably different way. In a first approximation we can note that the burst effect of modified samples decreases with decreasing amount of BTSE while the dissolution in the second part proceeds in a similar way for all modified samples.

The change of samples' morphology during the dissolution process was monitored by ex situ observation of selected samples under SEM and, additionally, using an "in situ" laser diffraction technique. The micrographs presented in Fig. 10 show that the nonmodified sample (no BTSE) dissolved quite uniformly leaving behind empty pores. In BTSE-modified samples, the dissolution was much less uniform. With increasing BTSE content a progressively rougher surface and even disintegration of the samples into flakes was clearly observed. This seems to be consistent with the more brittle nature of these samples. Disintegration of selected samples was quantitatively confirmed by particle size measurement (Fig. 11). The particle sizes of the nonmodified sample SCN1 did not change within the first 5 min of immersion (Fig. 11a). The particle size of modified samples, however, was rapidly decreasing within first 5 min of immersion (a representative graph for SCBN4 is shown in Fig. 11b). In the case of sample SCBN5 the disintegration occured within less than ca. 1 min of immersion and could not be followed using the present technique.

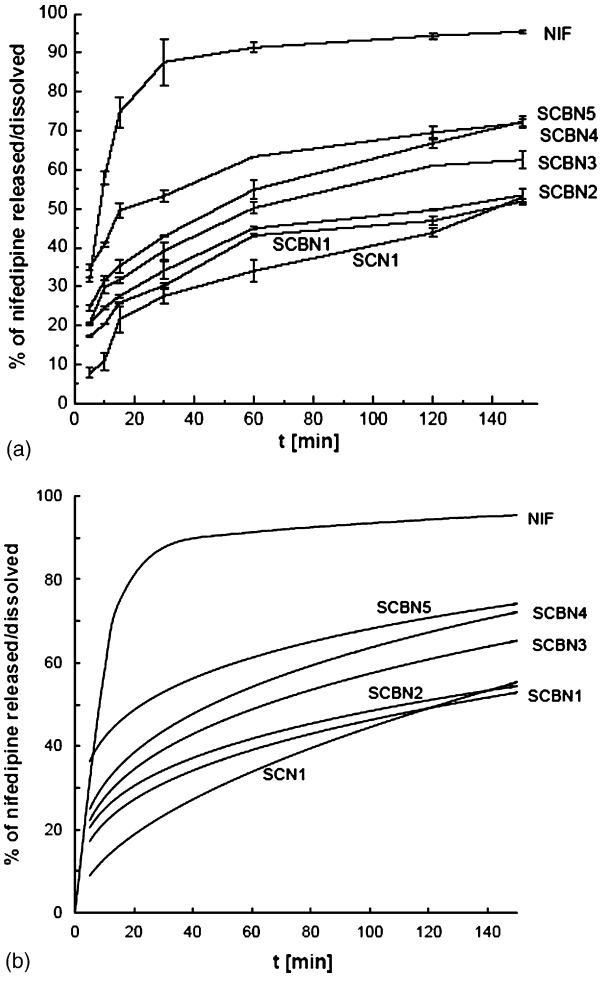

Fig. 9. (a) Percentage of NIF released as a function of time for the modified and nonmodified samples. For comparison, the dissolution of the pure free crystalline drug is also included. (b) Model curves obtained by a quantitative analysis of the measured dissolution curves. From 0 to 5 min only the part of NIF that was immediately set free due to partial silica disintegration in solvent is assumed to be dissolved (following the Noyes–Whitney law). After 5 min the release from the interior of xerogel was assumed to prevail (following Eq. (5)).

4. Discussion

The results of X-ray diffraction (Fig. 2) and thermal analysis (DTA and TG, Fig. 7) reveal consistently that NIF incorporated into the silica xerogel is completely amorphous. Although amorphous NIF has been successfully prepared by other authors

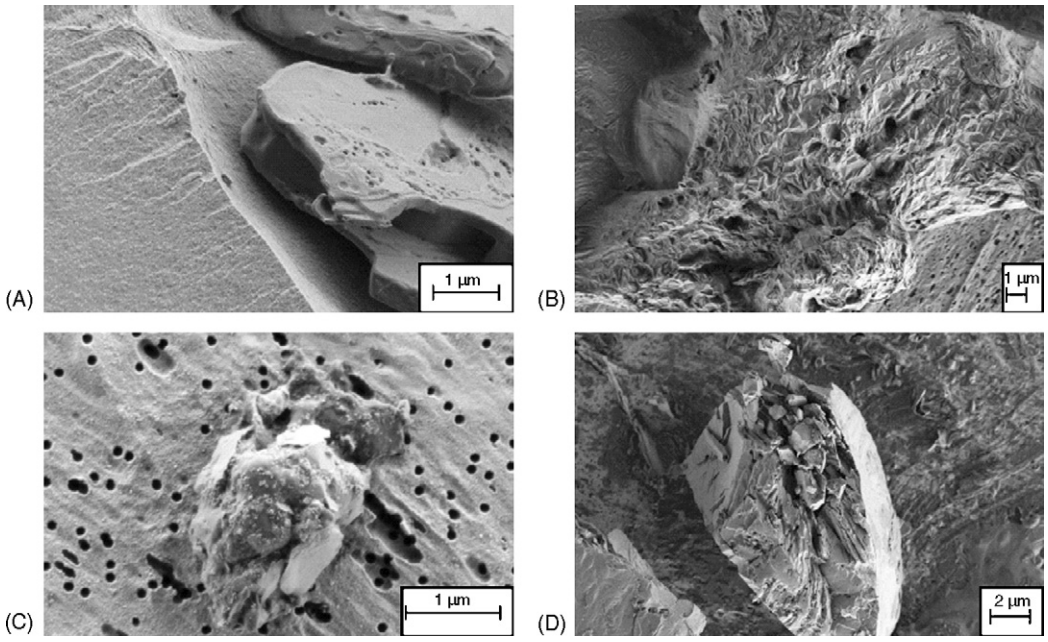

Fig. 10. Scanning electron micrographs after 5 min of release. (A) Nonmodified sample SCN1 (no BTSE), (B) modified sample SCBN4 (BTSE/TEOS mole ratio 0.3), (C) and (D) sample SCBN5 (no TEOS).

(Böttcher and Slowik, 1998), the resulting materials have not been temporally stable enough to achieve a therapeutical applicability. In the present case, NIF entrapped in the silica matrix remained in its amorphous form for at least 2 months (Fig. 2—sample SCBN1-2) (these measurements are still in progress).

We explain both the appearance of amorphicity and its temporal stability by assuming that the pores in the present silica carrier are too small to allow formation of critical nuclei needed for the crystallization process to start either from saturated solution or from the amorphous state—once formed. As shown elsewhere (Godec et al., 2006), such an assumption has a solid theoretical background. Here we only repeat the specific information needed for the present discussion.

The critical dimensions (r) of spherical and cubical nuclei needed for crystallization of NIF from a supersaturated solution can be calculated using the following two equations (Godec et al., 2006):

$$r^{\bullet\text{sphere}}_{\text{supersatur.}} = 2v_1 \frac{\bar{\gamma}}{kT \ln S} \tag{1}$$

$$r^{\bullet\text{cube}}_{\text{supersatur.}} = \frac{3\sqrt{3}v_1 \bar{\gamma}}{kT \ln S} \tag{2}$$

where v_1 is the monomer volume of drug, $\bar{\gamma}$ the average interfacial energy between the crystalline and the amorphous phase, k the Boltzmann's constant, T temperature and S is the supersaturation ratio.

Furthermore, the critical dimensions of spherical and cubical nuclei for crystallization from the amorphous phase are calculated from (Godec et al., 2006):

$$r^{\bullet\text{sphere}}_{\text{am.phase}} = -\frac{2\bar{\gamma}}{\Delta G_V} \equiv \frac{6C_T T_m^2 M \Delta H_{tr}}{(N_A V_m^2)^{1/3} \Delta T T \rho \Delta H_f} \tag{3}$$

$$r^{\bullet\text{cube}}_{\text{am.phase}} = -\frac{2\sqrt{3}\bar{\gamma}}{\Delta G_V} \equiv \frac{6\sqrt{3}C_T T_m^2 M \Delta H_{tr}}{(N_A V_m^2)^{1/3} \Delta T T \rho \Delta H_f} \tag{4}$$

where ΔG_V is the excess Gibbs free energy of the amorphous phase, C_T the Turnbull coefficient (for nonmetallic solids $C_T = 0.32$), T_m the melting temperature, M the molecular mass of NIF, ΔH_{tr} the enthalpy of the solid–solid transition (crystallization), N_A the Avogadro's number, V_m the molecular volume, T the temperature, $\Delta T = T_m - T$, ρ the density of NIF, and ΔH_f is the enthalpy of fusion.

The values of critical dimensions as calculated from Eqs. (1)–(4) are displayed in Table 3. It can be seen that all calculated values are significantly higher than the average dimensions of pores determined experimentally for the present silica matrices. In other words, the radii of pores in the present samples are too small to allow crystallization either from saturated solution or from the amorphous solid phase that has already formed within the pores.

Although, as the results confirm, all composites prepared in this study contain amorphous NIF, there are important differences in the composition and in the structure of individual samples. This may have an impact on their mechanical proper-

Table 3
Comparison of calculated and experimentally observed radii of crytical nuclei

	$r_{\text{experimental}}$ (nm)	$r_{\text{am.phase}}$ (nm)	$r_{\text{supersat.}}$ (nm)	
			$S = 1.5$	$S = 4.5$
Spherical nuclei	1.20	2.9	2.6	9.7
Cubical nuclei	1.44	4.5	6.8	24.4

$r_{\text{experimental}}$ is the average pore radius of the prepared samples, $r_{\text{am.phase}}$ is the radius of crystalline critical nuclei formed in the amorphous phase and $r_{\text{supersat.}}$ is the radius of the crystalline crytical nuclei formed in a supersaturated solution. S is the degree of supersaturation.

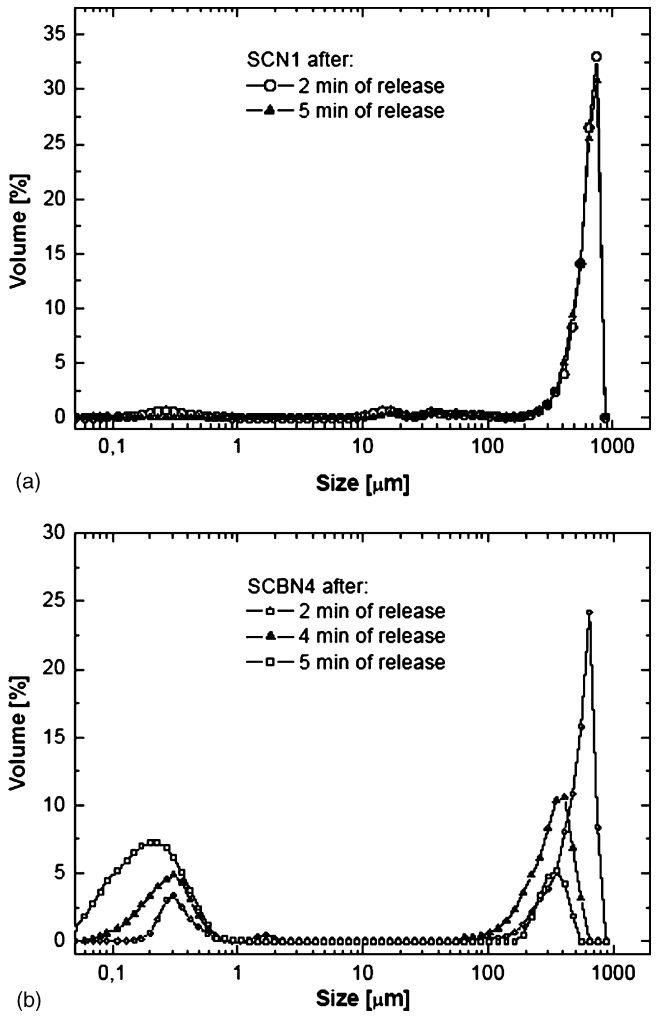

Fig. 11. Particle size analysis using laser diffraction. Prior to measuring, all samples were crushed and sown.

ties and, most importantly, on their behaviour during dissolution. As regards the formation mechanism of the prepared silicas, the absence of bands due to SiOEt in FTIR spectra indicates that in all samples the hydrolysis step has been completed. This is in agreement with previous studies by Bögershausen and coworkers on similar silica–drug composites who found that the slower step in the gelation process was the condensation step (Bögershausen and Koller, in press). There is, however, a difference in H_2O and EtOH content between different samples. As seen from the mass losses between 50 and 120 °C (Fig. 7), with increasing BTSE/TEOS ratio the H_2O and EtOH content decreases. This result is expected because EtOH and H_2O are inherently formed in the process of hydrolysis and condensation of TEOS. Addition of BTSE also affects the DTA and TG curves in the region between 190 and 250 °C (Fig. 7). We explain this by a decrease of surface SiOH in BTSE-modified with respect to the nonmodified samples, as also confirmed by analysis of FTIR spectra (Fig. 8): the intensity of the band at 950 cm^{-1}, which corresponds to vibrations due to SiOH groups, decreases with the increasing amount of BTSE. The content of SiOH groups could be very important for the dissolution behaviour because these groups increase the surface hydrophilicity and, thus, wettability in aqueous solutions. Here it should be noted that, unfortunately, the contact angle measurements could not be performed. Namely, capillarity due to porosity and high surface area of the samples was too high to measure the surface tension.

As mentioned in Section 3, we hoped that FTIR spectra would give insight into development of Si–O–Si bridges with changing BTSE/TEOS content. However, we found that the bands due to Si–O–Si bridges had two poorly resolved contributions in the associated peak appearing in the range 1200–980 cm^{-1}. Furthermore, addition of BTSE resulted in new contributions to this range. Due to interdependence of these contributions we were not able to quantify the effect of added BTSE on the Si–O–Si bridges.

Based on the differences in composition and structure of the prepared samples we try to explain the observed differences in dissolution curves. First, one expects intuitively that incorporation of a drug into pores of an insoluble solid matrix will suppress the dissolution rate of the drug. Indeed, as mentioned in Section 3, incorporation of NIF into nonmodified silica (SCN1) decreases the dissolution rate if compared to pure NIF (Fig. 9a). A quantitative analysis of the two curves even shows that the dissolution law changes from the Noyes–Whitney type for pure NIF to a power law type for SCN1. The suitability of power law for describing dissolution from homogeneous solid matrices has been demonstrated previously, both theoretically (Ritger and Peppas, 1987) and experimentally (Bögershausen and Koller, in press; Kortesuo and Ahola, 2001b). In general, the power law relates the amount of drug released per unit area, Q, and time of release, t, as follows

$$Q = kt^n \tag{5}$$

where k is a constant and n has a typical value of 0.5 for dissolution from slab-like geometries and slightly lower values for dissolution from spherical, cylindrical and other geometries (Ritger and Peppas, 1987). If the curve for sample SCN1 is fitted using Eq. (5) by taking k and n as variables, one gets for k a value of about 5.0 ± 1.1 (with t given in minutes and Q in percent of the total amount of NIF) and for n a value of about 0.46 ± 0.05, which agrees well with the theoretical predictions.

Analyzing the BTSE-modified samples with Eq. (5) gives unexpectedly large variations of the fitted parameters with the content of BTSE. For example, k increases from about 9 to 24 while power n decreases from 0.37 to 0.24 for samples SCBN1 to SCBN5, respectively. Such large parameter variations and, at the same, unusually low values of n cannot be explained by referring exclusively to the physical picture of release from homogeneous matrices (Ritger and Peppas, 1987). Based on the structural and microstructural properties of BTSE-modified samples, we assume that their release curves in Fig. 9a are a consequence of two consecutive and basically independent physical processes (see also schematics in Fig. 12): (a) the initial rapid increase in drug concentration (burst effect) is a consequence of an immediate mechanical erosion and/or disintegration of drug–carrier composites into smaller particles after immersion into solvent; such a material degradation was clearly observed by SEM and laser diffraction measurements (cf. Figs. 10 and 11 and

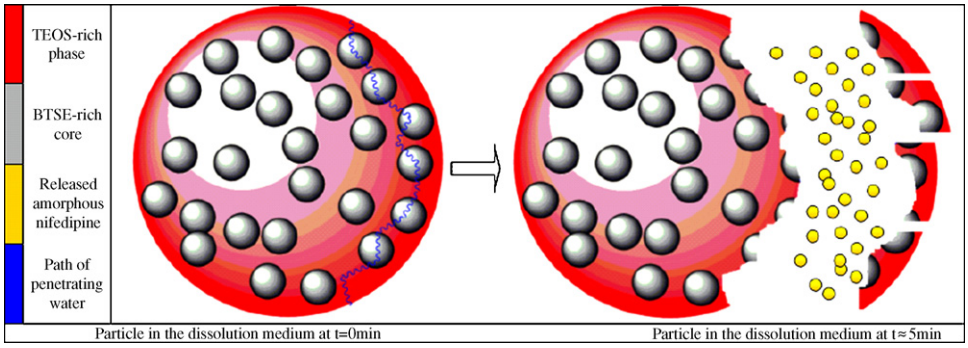

Fig. 12. Schematics of the proposed release scenario. Before immersion into solvent, all NIF (small yellow circles) is packed inside the matrix. The solvent partly breaks the xerogel matrix releasing a certain amount of NIF. This part dissolves rapidly while NIF that remains encapsulated is released slowly, according to Eq. (5). (For interpretation of the references to colour in this figure legend, the reader is referred to the web version of the article.)

the corresponding text). Upon this erosion and/or disintegration, considerable amounts of drug become directly exposed to the solvent and dissolve in the same way as pure NIF, i.e., according to the Noyes–Whitney equation; (b) after several minutes (5–10 min) the mechanical degradation of composites is stopped (as indicated by SEM and laser diffraction observations) leaving behind a considerable amount of eroded or smaller composite particles which still contain the incorporated drug. The release of this drug proceeds then according to Eq. (5).

We re-analyzed the dissolution curves in Fig. 9b by taking into account the proposed scenario. For BTSE-modified samples, Eq. (5) was applied only to the part of curves corresponding to dissolution times above 5 min, i.e., assuming that the release from the interior of xerogel matrices only began at that point. Such analysis gave quite good fits and much more reasonable values of model parameters. The fitted curves are displayed in Fig. 9b while the corresponding values of k and n (Eq. (5)) are listed in Table 4. Comparing the parameter values for all samples shows that k slightly increases and n slightly decreases with increasing BTSE content, apparently indicating a slightly faster drug dissolution from BTSE-rich samples. However, we estimate that these differences are too small to be conclusive, especially if the quite significant data scattering is taken into account. So, to a first approximation, one might say that the dissolution rate from the matrix interior is independent of the BTSE/TEOS ratio. In fact this result is quite surprising. Namely, after disintegration, the particles of BTSE-rich samples are in average much smaller than those in TEOS-rich samples (see Fig. 11). So, a much faster dissolution from the interior of the former is expected. Perhaps the effect of smaller volume is compensated by the increased hydrophobicity of the BTSE-rich samples. The latter is determined by the amount of surface sylanol groups, which as consistently shown by thermal analysis and FTIR spectroscopy, decreased by the increasing BTSE content.

Table 4
The values of parameters k and n and their standard deviations from power law fitted dissolution curves, which were corrected for the burst effect

	k (s^{-1})	S.D. (k) (s^{-1})	n	S.D. (n)
SCN1	4.51	1.42	0.49	0.07
SCBN1	3.69	1.66	0.49	0.11
SCBN2	3.68	1.63	0.48	0.11
SCBN3	5.93	2.03	0.43	0.08
SCBN4	4.77	1.66	0.50	0.08
SCBN5	6.16	2.04	0.39	0.08

Most significant differences between the samples appear in the initial stage of drug dissolution (after 5–10 min). The increasing dissolution rate with increased BTSE content can be linked to the increasing brittleness of the samples. Partly, this can be explained by the fact that BTSE particles can only grow in three directions in space, as opposed to the possibility of a four-direction growth in samples containing solely TEOS (or smaller amounts of BTSE)—due to the four hydrolizable-OEt groups (schematically shown in Fig. 1). It is also known that degradation of porous silica xerogels occurs through hydrolysis of the Si–O–Si through the entire network (Brinker and Scherer, 1990; Czuryszkiewicz et al., 2002; Tamada and Langer, 1993). Despite the difficulties in detection of Si–O–Si bridges (see Section 4), we estimate that also in the present samples the siloxane bridges play an important role in the dissolution process. In particular, we assume that the Si–O–Si bridges between the primary BTSE-rich core and the TEOS-rich phase are especially prone to hydrolysis. It is probably in this region of increased disorder that the silica matrix breaks most easily.

5. Conclusions

We prepared a range of silicate-based xerogels containing amorphous NIF. No crystallization was observed for a period of more than 6 months (the experiment has not been finished as yet). The occurrence and stability of amorphous NIF are explained by the fact that NIF is spatially constrained within pores of an average size of about 2.4 nm while for crystallization a space larger than ca. 3.4 nm (in diameter, if spherical) is theoretically predicted. The proposed procedure can in principle be expanded to other drugs where amorphicity is the preferred state, either due to patent protection of the crystalline analogues or due to pharmaceutical advantages of the amorphous form, like higher solubility.

The structural and mechanical properties of the prepared xerogels were controlled by varying the molar ratio between two silicate precursors: tetraethoxysilane (TEOS) and (bis-1,2-(triethoxysilyl)ethane, BTSE). With increasing BTSE content the samples became more brittle and degraded faster when

immersed into a solution. Hence, using appropriate TEOS/BTSE ratio we could partly tailor the drug release profile: the brittler the samples the more expressed was the initial burst effect. In all cases, the burst effect was followed by a much slower (power law) drug release. Such "two-rate release pattern" could be used in all cases in which we wish to achieve a controlled release with an initial burst. This way, we achieve a predetermined plasma concentration that can be maintained via the subsequent diffusion of the incorporated drug out of the insoluble matrix. Alternatively, one could use such composites to suppress the dissolution and absorption rate in cases where too high rates could lead to toxic side effects.

Acknowledgments

Financial support from The Ministry of Higher Education, Science and Technology of the Republic of Slovenia, the National Institute of Chemistry and the Faculty of Pharmacy is gratefully acknowledged.

References

Anderson, J., Rosenholm, J., 2004. Influences of material characteristics on ibuprofen drug loading and release profiles from ordered micro-and mesoporous silica matrices. Chem. Mater. 16, 4160–4167.

Böttcher, H., Slowik, P., 1998. Sol–gel carrier systems for controlled drug delivery. J. Sol–Gel Sci. Technol. 13, 277–281.

Bögershausen, A., Koller, H., in press. Drug release from self-assembled inorganic–organic hybrid gels and gated porosity detected by positron annihilation lifetime spectroscopy. Chem. Mater.

Breimer, D.D., Danhof, M., 1997. Relevance of the application of pharmakokinetic–pharmakodynamic modelling concepts in drug development. Clin. Pharmacokinet. 32, 259–267.

Brinker, C.J., Scherer, G.W., 1990. Structural changes during heating: amorphous systems. In: Sol–Gel Science: The Physics and Chemistry of Sol–Gel Processing. Academic Press, New York, pp. 547–615.

Budvári-Báráni, Z., Szász, G., 1990. Some new data concerning the chromatographic purity test for nifedipine. J. Liquid Chromatogr. 13, 3541–3551.

Curran, M.D., Stiegman, A.E., 1999. Morphology and pore structure of silica xerogels made at low pH. J. Non-Cryst. Solids 249, 62–68.

Czuryszkiewicz, T., Ahvenlamni, J., Kortesuo, P., Ahola, M., 2002. Drug release from biodegradable silica fibers. J. Non-Cryst. Solids 306, 1–10.

Franquet, A., Biesemans, M., 2004. Multinuclear 1D- and 2D NMR study of the hydrolysis and condensation of bis-1,2-(triethoxysylil)ethane. J. Adhesion Sci. Technol. 18 (7), 765–778.

Godec, A., Maver, U., Bele, M., Planinšek, O., Gaberšček, M., Srčič, S., Jamnik, J., 2006. Vitrification from solution in restricted space-formation and stabilization of amorphous nifedipine in a silica xerogel carrier. J. Pharm. Sci., submitted for publication.

Hu, Y., Mackenzie, J.D., 1992. Mater. Res. Soc. Symp. Proc. 271, 681.

Jain, R., Shah, N.V., 1998. Controlled drug delivery by biodegradable polyester devices: different preparative approaches. Drug. Dev. Ind. Pharm. 24, 703–727.

Kortesuo, P., Ahola, M., 2001a. In vitro release of dexmedetomidine from silica xerogel monoliths: effect of sol–gel synthesis parameters. Int. J. Pharm. 221, 107–114.

Kortesuo, P., Ahola, M., 2001b. Alkyl substituted silica gel as a carrier in the controlled release of dexmedetomoidine. J. Control. Rel. 76, 227–238.

Krihak, M., Shahriari, M.R., 1996. The effect of MTMS on the optical properties of TEOS syntesized gels doped with thionin. Opt. Mater. 5, 301–310.

Melde, B., Holland, B., 1999. Mesoporous sieves with unified hybrid inorganic/organic frameworks. Chem. Mater. 11, 3302–3308.

Nicoll, S.B., Radin, S., 1997. In vitro release kinetics of biologically active transforming growth factor-1 from novel porous glass carrier. Biomaterials 18, 853–859.

Ritger, P.L., Peppas, N.A., 1987. A simple equation for description of solute release. I. Fickian and Non-Fickian release from non-swellable devices in the form of slabs, spheres and cylinders or discs. J. Control. Rel. 5, 23–36.

Ro, J.C., Chun, I.J.G., 1991. Structures and properties of silica gels prepared by the sol–gel method. J. Non-Cryst. Solids 130, 8–17.

Rösler, A., Vandermuelen, G.W.M., 2001. Adv. Drug Deliv. Rev. 53, 95.

Santos, E.M., Radin, S., 1999. Sol–gel derived carrier for controlled release of proteins. Biomaterials 20, 1695–1700.

Syed Laik, A., 1989. Nifedipine.Nifedipine. In: Florey, K. (Ed.), Analytical Profiles of Drug Substances, vol. 18. Academic Press, New York, pp. 221–288.

Tamada, J.A., Langer, R., 1993. Erosion kinetics of hydrolytically degradable polymers. Proc. Natl. Acad. Sci. USA 90, 552–556.

The MERCK Index, 2001, 13th ed., Merck & Company Incorporated, Whitehouse Station, New Jersey, USA.

Unger, K., Rupprecht, H., 1983. The use of porous and surface modified silicas as drug delivery and stabilizing agent. Drug. Dev. Ind. Pharm. 9, 69–81.

Wagh, P.B., Pajonk, G.M., 1997. Influence of temperature on the physical properties of citric acid catalyzed TEOS silica aerogels. Mater. Chem. Phys. 50, 76–81.

Wagh, P.B., Venkateswara Rao, A., 1998. Influence of mole ratios of precursor, solvent and water on physical properties of citric acid catalyzed TEOS silica aerogels. Mater. Chem. Phys. 53, 4147.

Watanabe, T., Wakiyama, N., 2001. Stability of amorphous indometacin compounded with silica. Int. J. Pharmaceut. 222, 81–91.

Wu, Z., Joo, H., 2004. Design of doped hybrid xerogels for a controlled release of brilliant blue FCF. J. Non-Cryst. Solids 342, 46–53.

Wu, Z., Joo, H., 2005. Controlled release of lidocaine hydrochloride from the surfactant-doped hybrid xerogels. J. Control. Rel. 104, 497–505.

Yang, H.S., Choi, S.Y., 1999. Thin Solid Films 348, 69.